BNL-105834-2014-TECH

EP&S No. 119;BNL-105834-2014-IR

Ultraprecise magnet deesign and shimming studies

G. T. Danby

April 1987

Collider Accelerator Department

Brookhaven National Laboratory

U.S. Department of Energy

USDOE Office of Science (SC)

DISCLAIMER

Internal Distribution

BROOKHAVEN NATIONAL LABORATORY
Associated Universities, Inc.
Upton, New York 11973

AGS/EP&S Tech. Note No. 119

ULTRAPRECISE MAGNET DESIGN AND SHIMMING STUDIES* **

G.T. Danby and J.W. Jackson

April 13, 1987

Abstract

Computer studies of pole design and magnet shimming techniques are discussed for a very precise 14.72 kG iron core storage ring magnet to be used for the proposed measurement of the muon anomalous magnetic moment. The experiment requires knowledge of the field in the 7m radius storage ring dipole to approximately 0.1 ppm (1×10^{-7}). The goal is to produce field uniformity of approximately 1 ppm. Practical and mathematical limitations prevent obtaining such accuracy directly with a computer code such as POISSON, which is used in this study. However, this precision can be obtained for perturbations of the magnetic field. Results are presented on the internal consistency of the computations and on the reliability of computing perturbations produced by Fe shims. Shimming techniques for very precise field modification and control are presented.

I. Introduction

This report, limited in its scope to computer studies by the authors, discusses a part of the ongoing design effort for an ultraprecise 3 GeV/c storage ring. The g-2 experiment proposal[1,2] has been approved as part of the future physics program at the high intensity, post- Booster, Alternating Gradient Synchrotron (AGS). An international collaboration is involved in detailed design of the storage ring and detection apparatus.

The computer studies are of general interest because of the precision required. Most accelerator magnets perform at a $\Delta B/B_o \geq 1 \times 10^{-4}$ field uniformity, for which the computer codes--in this instance POISSON[3]--can, if carefully used, reliably predict the field within the beam aperture. For example, the AGS Booster dipoles agreed with computations to $\Delta B/B \sim 1 \times 10^{-4}$ over the "good field" aperture. High field superconducting magnets designed by the authors have also shown agreement to this precision.

---

* Work performed under the auspices of the U.S. Dept. of Energy.

** This is an expanded version of a Paper prepared by the authors for the 1987 IEEE Accelerator Conference on computer design studies for the g-2 storage ring magnet.

The experiment and the storage ring design are solidly based on a highly successful CERN design.[4,5] This was the third of a series of muon g-2 experiments carried out at CERN and resulted in a knowledge of the magnetic field integral appropriately averaged over the muon orbits to $\Delta B/B_o$ = 1 to 2 x 10^{-6}. This plus other smaller systematic errors were less than the statistical uncertainty of 7 PPM obtained in the experiment. The result stands as the state of the art.

After commissioning the Booster, operation at 5 x 10^{13} protons in the AGS should permit a statistical uncertainty of only 0.3 PPM in the new experiment, assuming the same pion decay injection technique as at CERN. Other injection possibilities might further reduce this error, i.e., direct muon injection and "exotic" beam front end optics. To carry out this very fundamental measurement, it is desirable that systematic errors be ≤0.1 PPM. These are dominated by magnetic field uncertainty, which involves the error in knowledge of the magnetic field, averaged over space and time in relation to the muon distribution. Field measurement errors also contribute. Figure 1 taken from the 1986 update[2] of the Proposal shows the general layout of the experiment. Figure 2 shows the magnet cross section in the 1985 version and Figs. 3 and 4 the 1986 updated version.

The new g-2 collaboration has not found a conceptual approach to the experiment superior to CERN 3. The polarized muons were captured in a uniform field (circular orbits) with weak vertical focusing provided by electrostatic quadrupoles. At γ magic=29.3 (3.094 GeV/c) the electric field drops out of the precession to first order. The high precision comes from being required "only" to produce and measure a very uniform magnetic field.

At CERN a ring of iron C-magnets [B_ρ = 14.72 kG x 7m] was used, with a 14-cm gap, open towards the inside radius with essentially continuous circumferential counters to detect the daughter electrons.

After considerable study of "table top" superconducting storage rings [$B_\rho \simeq$ 5T x 2m] the new g-2 collaboration decided in early 1985 for various technical, theoretical and practical reasons to concentrate on an iron dominated, C-magnet approach and submit a proposal in the autumn of 1985. CERN had used a "polygon" of 40 magnet yokes, joined together into a continuous ring at the pole region. It was decided the new ring would have a larger gap, 18 cm, since much more elaborate field monitoring and control seems necessary to attempt a factor of 20 improvement. A "continuous" ring magnet rather than polygon yoke sections was also chosen.

The preliminary engineering drawings of the magnet for the Proposal[1] were prepared at MIT. This included the layout of the steel and the design of the superconducting excitation coils for the iron ("superferric") magnet. The authors of this report provided precision design of the polar region and other refinements to the magnet in the Proposal.[1]

Following a favorable formal physics review in the autumn of 1985, during 1986, a larger collaboration, refined the magnet design considerably. The participants were principally from Brookhaven, Boston and Yale Universities. Solicitations were made to industry for the iron portions of the magnet. This considerably improved the cost credibility of the experiment, since the iron yoke dominates the storage ring cost.

In late 1986 the experiment was again reviewed and was approved.

This brief historical outline does not do justice to the contributions to the storage ring magnet parameters and design by various members of the collaboration. It is a complex experiment, with many interacting components to be accommodated.

The improvements in precision anticipated for the new experiment come from several areas:

(i) The gap increase from 14 to 18 cm allows for more elaborate field monitoring and feedback. For CERN the principal error[4-5] was control of each of the 40 magnet sections by correction coils. These used feedback from a single point NMR measurement in each section. With extra space much more elaborate control can be used.

(ii) A "trolley" capable of moving around the circumference inside the beam aperture carrying a matrix of NMR probes is being constructed. This can be "parked" out of the way without breaking vacuum. This "on-line," albeit intermittent, coexistence of complete mapping and physics running is a new feature.

(iii) The "end effects" of the CERN 40 magnet blocks, although semicontinous, contributed significant field and measurement errors between blocks. The new ring will be constructed with 45° sectors machined to be close fitting at their ends. This should be a much closer approximation to a continuous ring.

(iv) More elaborate use of field shimming by adjusting the iron cross section remote from the pole faces is planned. In fact, a large air gap between the pole and the return yoke will be used as part of this strategy.

(V) The use of superconducting (SC) excitation is a significant change. SC coils are extremely attractive for field and ripple control, because of the high Q and low voltages required. A well insulated cryostat also ensures minimal thermal interactions with the iron.

It must be noted that CERN took extreme care with their copper coil design to minimize interaction of coil and iron. It is not clear at what level their coils presented a limitation. Nevertheless SC excitation appears to have the edge.

CERN required elaborate magnet cycling and a long settling time before physics running. It is hoped with SC coils the magnet can stay on indefinitely because of low power requirements. This is perhaps the most important reason for using SC coils. Operation will also be much less vulnerable to power dips, a common problem at BNL. Cycle changes can be dictated solely by the needs of the experiment.

The larger magnet gap and the increased reluctance due to the air gaps behind the poles result in higher ampere turns. These requirements are still very small by the standards of SC coils. (This will be demonstrated later in Table V.)

The goal of the computer simulations has been to develop techniques to control the dipole field and lower order multipoles so that $\Delta B/B \leq 1 \times 10^{-5}$ over the necessary "good field" 9 cm diameter can be relatively easily obtained. The error would be reduced to $<1 \times 10^{-6}$ by special local static shimming or by active current control such as pole face windings. The final factor of 10 to $\Delta B/B < 1 \times 10^{-7}$ would come from measurements i.e., knowledge of the field adequate to compute the orbits over the muon distribution.

The calculations have already produced a good precision pole profile, although not a final one. Further work on the pole is required. Only part of the final design can be performed by calculation. The following lists some other questions.

1. Can specialty steel produce more homogeneous pole surface regions, freer of inclusions or voids which may cause "potholes" in the field?

2. Will grinding or polishing of pole plates of reasonable size result in greater planarity of pole surfaces at reasonable cost? (The surface fine structure does not require a mirror finish.)

3. Are higher performance magnet steels warranted, at least in some small portions of the pole profile?

An experimental program is planned in the near future. A modified general purpose beam transport magnet will be used as the flux return. The polar regions will be modeled in exact scale. Materials studies will be carried out, as well as experimental shimming on the pole surfaces and in the air gaps behind the poles. Measurement and field control techniques will also be studied.

II. Design Optimization

During 1986 the computer calculations were used to reduce the cross section and weight of the magnet to 2/3 that in the Proposal.[1] The introduction of 1 cm "air" gaps between each pole and return yoke facilitated this, since the reluctance of the flux return is significantly decoupled from the behavior of the poles. (See Table I.)

TABLE I: Multipole Change with Air Gap and Weight Reduction.
B = 14.7 kG

	I Base* (W = 65cm)	II W = 55 cm	III W = 55 cm +4 corners off	IV W = 55 cm +4 corners off +10 cm off
$\Delta NI/NI$(base)	0	+2.16%	+2.40%	+4.30%
$\Delta B_n/B_o$	(Normalized)			
n = 1 (quad)	0	-1.3 PPM	-2.6 PPM	-2.6 PPM
2 (sext)	0	- .6	- .5	- .7
3	0	- .1	- .1	- .1
4	0	0	0	0
5	0	0	0	0
6	0	0	0	0
7	0	0	0	0
8	0	0	0	0

Col. I: the 1985 Proposal Magnet Cross Section, changed to add 1 cm air gap behind each pole.

Col. II: for a 10 cm (18%) reduction in width W of the return yoke block which is centered on the horizontal midplane. (See Fig. 2.)

Col. III: also cut four corners off the magnet.

Col. IV: the changes of Col. II plus Col. III and also reduced thickness of top and bottom yoke members by 10 cm. (This increased reluctance by ~2%.)

In all cases in this Report, multipoles are expressed at R = 4.5 cm, y = 0; B_o = 14.7 kG.

The result of very large return yoke weight (and cost) reduction is an appreciable increase in reluctance and ampere turns requirement, but no significant change in multipole field errors. The magnetic and dimensional tolerances of the yoke flux return are not unusually tight and are relevant mainly to the dipolar term. As an example, scaling from Col. II, a 0.65 mm change in width of the HMP block would produce dipolar change of 1.4×10^{-4}. This is the same as the effect of a change of 25 μm in the 18 cm gap.

Consider now the effect of raising the central field by 1% in two cases, the geometry of Col. I and of Col. IV in Table I. This result is shown in Table II.

TABLE II: Change for B_o increased by 1% to 14.847 kG.

	I (Base, 1985)	II (light weight)
$\Delta NI/NI$	1% + 0.16%	1% + 0.58%
$\Delta B_n/B_o$ (4.5 cm)		
n = 1 (quad)	-14.2 PPM	-14.7 PPM
n = 2 (sext)	-6.6	- 6.8
n = 3	- .2	- 0.2
n = 4	- .3	- 0.3
n = 5	0	0
n = 6	0	0
n = 7	0	0
n = 8	0	0

Note the effect on the field multipoles of raising B_o by 1% is almost independent of the very large changes in yoke geometry. The quadrupole is due to C-magnet yoke assymetry. The 1% higher field reduces the permeability in the vicinity of the air gaps.

The reduced permeability in the poles also effects the sextupole.

Table II can also be used to establish tolerances on magnetization properties in the pole steel. A 1% change in saturation magnetization would produce roughly the multipole change in Table II. The storage ring central field will not be changed from 14.72 kG in operation.

The C-magnet return produces a very large systematic gradient to be corrected. Three perturbations have been explored: (i) tilt the pole faces, (ii) larger bumps on the inside pole edges than on the outside, (iii) shim in the air gap at the rear of the poles to induce more flux on the inside. While (i) and (ii) are possible for refined shimming, they are too local to the "good field" aperture and generate significant octupole. Method (iii) can give a large almost pure quadrupole so the magnet can start off with the systematic C-magnet gradient removed. This is shown in Table III.

TABLE III. Perturbing Air Gap Behind Pole to Remove Quadrupole.

$\Delta B_n/B_o$ (4.5 cm)	I "Standard" Case	II Pole gap Slope ±0.40 cm	III Effect of "wedge" gap
n=1(quad)	-204.6 PPM	+ 3.4 PPM	+208 PPM
n=2(sext)	- 38.9	-32.8	+ 6.1
3	+ 1.7	- 1.1	- 2.8
4	- 0.2	- 0.5	- 0.3
5	+ 0.2	+ 0.2	0
6	- 1.3	- 1.3	0
7	- 0.2	- 0.2	0
8	- 0.2	- 0.2	0

Col. I: standard case (see Fig. 3) 1 cm air gap.

Col. II: base of pole wedged so that air gap varies from 1.4 cm at R = +28 cm to 0.6 cm at R = -28 cm. This effect can be accomplished also by moving the center of gravity of shims in the parallel air gap.

Col. III is the difference between II and I.

Note the almost pure quadrupole, with only 1% octupole contribution. A small sextupole change occurs as a breakdown of symmetry because of the very large radial asymmetry being corrected. This simply becomes part of the baseline gradient corrected magnet.

The effect of the coil motion is shown in Table IV.

TABLE IV: Coil Position Tolerance

n	Multipole (4.5 cm)	Outer Coil Up 1 mm.	Outer Coil Inward 1 mm.
0	Dipole	- 24.1 PPM	+ 7.56 PPM
1	Quadrupole	+ 0.60	+ 0.38
2	Sextupole	- 0.09	- 0.12
3	Octupole	+ 0.02	+ 0.04
4	Decapole	- 0.01	- 0.02

Notes:
1. Outer coils are located at R = 739 cm, y = ±15 cm (Fig. 2 and Fig. 3.)

2. Inner coil not tabulated but sensitivity less.

3. All multipole terms < 1 PPM, except for dipole.

Note that absolute coil position is not critical to field quality. This is helpful considering the very large size of the coil rings and their relatively small cross sections.

Several millimeters of permanent displacement could be tolerated. Even non-reproducibility of position with thermal or magnetic cycling at the millimeter level looks tolerable providing the field is mapped after excitation and before physics running. This requires a constant position during actual running, or else feedback correction with coils.

During 1986 the location of the inside coils was changed from y = ± 23cm to Y = ± 30cm. This change permitted access to the air gap behind the pole for shimming. In addition, it resulted in approximately zero radial force. The original location had a negative magnetic hoop stress on the inner coils, a bad situation. The increase in stored energy and ampere turns was extremely small for this change.

Figure 5 shows the computed forces on the coils and also on the various portions of the magnet steel.

Note that the poles are each attracted to their adjacent yokes by 800 lbs/linear inch. This is for the lcm air gap case shown in Fig. 3. The sign of this force and its modest strength is very attractive from a support point of view.

The sensitivity of the force computations to steel properties was explored. Table V shows the forces on the coils and on the poles for realistic iron permeability for low carbon steel, and also for $\mu = 10{,}000$ and $\mu = \infty$ in the iron. These were calculated for a tapered air gap to remove the quadrupole (as in Table III). As a result, the forces on the pole are slightly different than in Fig. V for real permeability.

The very large but finite $\mu = 10{,}000$ computations show coil forces only slightly smaller than low carbon steel. Further increase to $\mu = \infty$ shows very small additional force change. The fields experienced by the coils are dominated by the air gap reluctance involved, so are weakly dependent on the detailed steel properties.

The force of attraction of the poles to the top and bottom yoke pieces increases slightly for $\mu = 10{,}000$, The $\mu = \infty$ results for pole forces are significantly different. Since the pole forces are much more iron dominated than the coil forces, this is not surprising.

Table V demonstrates that the use of special magnet steels (much more expensive) in the polar region would have only a minor effect on forces.

TABLE V: Forces at B_o = 14.72 kG as a function of permeability

	Force Components	Inner Coil	Outer Coil	Pole
$\mu = \infty$	F_x	10.1	-189.7	20.0
	F_y	134.5	134.3	1880.0
$\mu = 10{,}000$	F_x	10.1	-191.1	74.2
	F_y	135.4	135.2	1041.0
μ = REAL	F_x	7.45	-204.8	64.0
	F_y	142.0	140.6	847.9

Note: Forces are expressed in Lbs/Linear inch at R = 7 meters.

Table VI shows the ampere turns per coil for real permeability, and for $\mu = 10{,}000$ and $\mu = \infty$.

TABLE VI: Ampere-turns and stored energy at $B_o = 14.72$ kG as a function of permeability

Permeability	NI/coil (kAt)	$NI/NI_{\mu=\infty}^{*}$	W (MJ)	$W/W_{\mu=\infty}^{*}$
∞	118.2498	1	5.611	1
10,000	118.4472	1.00167	5.653	1.00173
Real	131.6970	1.11372	6.296	1.1174

* Normalized to $\mu = \infty$ value.

The reluctance of the iron portions of the magnet increase the ampere turns required by 11.4% compared to $\mu = \infty$.

If the magnet had no air gap behind the poles, the ampere turns per coil would be 105.4242 kA T for $\mu = \infty$. Thus, adding the additional air gap has raised the ampere turns by 12%. This small increase will also roughly apply to stored energy and coil forces.

The stored energy W in the ring is also listed. Note that normalized to $\mu = \infty$, the stored energy with real permeability is 11.7% larger. This is very similar to the increase in ampere turns.

III. Shimming Perturbations

The approach of the g-2 design is to produce pole surfaces as flat as economically practical by machining plus possibly grinding or polishing the surface of sections to minimize "hill and dale" errors. Very homogeneous material will be used to minimize "pot holes."

For reference, consider artificially simplified 0.001" (25 μm) errors in the gap and the parallelism of the pole surfaces: (i) a .001" systematic gap error gives $\Delta B_o/B_o = 141$ ppm dipole change, (ii) a .001" side-to-side tilt of two plane pole surfaces gives a quadrupole of 11 ppm at R = 4.5 cm, the good field aperture limit, (iii) a .001 symmetric variation, i.e. let the gap at the center be .001" different than at both pole edges, will give ~ 3.6 ppm sextupole. The above illustrates the incentive to make the dipole $\Delta B_o/B_o$ very small around the azimuth by shimming the reluctance or possibly also by current loops remote from the pole surfaces.

The present state of the design is shown in Col. II of Table III. All terms are small except for the 33 ppm sextupole. A slight change to the symmetric pole profile will be required to remove the sextupole. Slight touchup of radial asymmetry can take care of quadrupole and octupole components in the computed magnet.

The perturbation studies carried to this level of accuracy serve only to illustrate techniques for optimization: the magnet as first constructed will in all probability have larger error terms than those computed. Systematic errors in the computed magnet will be discussed in the next section. As emphasized earlier, the results are sufficiently correct to serve as a valid basis for design and for perturbations.

Tests of internal consistency of computations (in ascending order of complexity) are:

(i) The field is computed in the "good field" aperture region, using realistic permeability data. A multipole fit is derived from the computed field and used to reconstruct the field. (See Fig. 6.) This test of "internal arithmetic" is important--multipoles are a very powerful tool to the magnet designer.

(ii) A portion of the magnet iron is perturbed and the multipole change is computed. The amplitude only of the iron change is then varied. Over a wide but reasonable amplitude range a linear relationship to the amplitude of the resulting multipole content is found. This perturbation can then be extrapolated.

(iii) Predictions from symmetry. A bump change is imposed on one of the four corners of the poles and the multipole change is computed. Symmetry predicts this bump change will produce equal amplitudes of multipole changes when applied to any or all of the four quadrants, with predictable phase changes. The magnet is computed with various combinations of up to four bumps of either sign (adding or subtracting iron). The agreement with prediction is excellent over a wide range of bump amplitudes.

Next to the pole faces themselves, the most sensitive perturbations are the bumps on the edges of the pole faces. In the present design these are 0.5 cm thick and 6 cm wide, extending from R = ±15 cm to R = ±21 cm. Their tolerances and their utility for perturbations are shown in Table VII.

TABLE VII. Perturbation of Bumps on Pole Face Edges.

B_n/B_o (4.5)cm	I Add .02 cm to inner bumps	II Add .02 cm to outer bumps	III Predicted Sum	IV Computed Sum
n=1 (quad)	+18.0	-18.4	- 0.4	- 0.7
2 (sext)	+14.9	+15.1	+30.0	+30.1
3 (oct)	+ 7.9	- 7.7	+ 0.2	+ 0.1
4	+ 2.9	- 2.9	5.8	5.8
5	+ 0.8 + 0.2	+ 0.8 + 0.2	0 + 0.4	0 + 0.4

In Col. I and II, the field has been computed for the thickness of the two bumps increased at the inner and outer radius respectively. Column III is the analytic sum of I and II. Column IV is the computed field sum, i.e., .02 cm added to the thickness of all four bumps.

Note that Col. IV shows a calculated symmetric perturbation and gives only symmetric terms. The ratio of 10 pole to sextupole is 20%. This bump perturbation should be used in combination with a more remote perturbation to suppress both sextupole and (n=4) 10-pole components simultaneously.

Subtracting Column II from Column I shows that if antisymmetric equal and opposite sign changes were made on the inside and outside radius bumps (i.e. add iron to inner bumps and remove iron from outer bumps), the sextupole would not change, only quadrupole and other odd terms. This bump change is a good way to reduce the octupole field. The residual gradient is removed by other means. (See Table III.)

Table VII permits estimating bump tolerances. For example, .001" (25 μm) rms bump height errors give 2 ppm sextupole and 2 ppm quadrupole. Everything else is smaller. Skew moments (not computed) will be comparable.

The magnet as first assembled will have significant deviations from computed predictions. These will be due to geometrical tolerance factors, structural response to magnetic forces, iron magnetization plus eddy currents, temperature control, etc. (An error $\Delta B/B_o$ of 1 ppm $\equiv$ 0.18μm change in an 18 cm gap.)

Except for localized errors at the pole surfaces, the perturbation calculations can be used to predict the necessary geometric corrections, i.e. passive shims. Note that computations will themselves add a small systematic error, for example, errors due to finite boundary conditions. These systematic errors can be treated like the practical construction errors, i.e. something to be removed by computer-predicted corrective perturbations of the residual magnet error.

At some level, temporal variations and cyclical non-reproducibility will become dominant even with very careful cycling and control. This residual error must be corrected by many servoed correction coils, perhaps by using coil sets 1 m long.

Dynamic dipole correction coils can be located off the pole face. This will minimize generation of heat on the poles. Valuable pole face space will be conserved. Field errors generated by the coils themselves will be minimized.

Pole face windings are analytically straightforward, but should be used only for small corrections. The current distributions are lumpy and generate higher order multipoles while correcting the desired field term. These errors are typically several percent as large as the basic term. The final ampere turn ensemble on the pole faces must have acceptably small higher moments since these are included in the $\Delta B/B_o \leq 0.1$ ppm knowledge of the field finally required during physics data taking.

IV. Systematic Effects Impacting on the Computer Predictions

(a) The computations made depend on a realistic but single valued permeability table which gives μ as a function of H. The actual iron is subject to hysteresis. The alignment of the domains in the magnet constitutes a many-body problem. Their response involves not only the coil ampere-turns, but very strongly their mutual interactions. The previous excitation history, both B and $\dot{B}$ (magnetization and eddy currents), affects the resultant field.

With careful excitation control, errors of reproducibility can be kept very small. The experience of the authors (and of others) that agreement at the 1×10^{-4} level can be achieved really applies to multipoles, i.e., to field shape. By far the largest magnetization effect is in the dipole term itself, B/I. This is normally not critical as long as it is homogeneous. This is the case in the g-2 ring, uniformity of B/I around the ring is what is required to great precision, not the absolute value.

(b) The precision perturbations demonstrated as well as the absolute field shape predictions depend on careful use of the POISSON Code.

A very important consideration is the effect of the convergence criteria (R/L) on the computed field and computed field harmonics. The R/L parameter tests the convergence of the potential solution of air, interface and iron points with 5×10^{-7} being the default value in POISSON. However for the purpose of designing the ultraprecise g-2 magnet it was found to be necessary to reduce the convergence criteria by several orders of magnitude in order to obtain the required internal consistency of ≤ 0.1 PPM in the computations.

Table VIII shows the effect of variation of R/L for a recent magnet geometry calculation. The value $R/L = 5 \times 10^{-9}$ used herein is clearly in a plateau, both for obtaining the multipole content and for successfully reproducing the calculated field at r = 4.5 cm. The quantity, σ, is defined as the difference between the multipole reconstructed field and the computed field (Fig. 6.).

TABLE VIII: Impact of convergence criteria on computed field and on multipole reproduced field.

R/L =	5×10^{-7}	5×10^{-8}	5×10^{-9}	5×10^{-10}
n = 1	-3.17 ppm	-0.34 ppm	-0.08 ppm	-0.06 ppm
2	+7.55	+7.18	+7.15	+7.15
3	-0.93	-0.33	-0.27	-0.27
4	+8.44	+8.37	+8.36	+8.36
5	+0.12	+0.30	+0.32	+0.32
6	-0.55	-0.57	-0.57	-0.57
7	-0.07	-0.01	-0.00	-0.00
8	-0.22	-0.23	-0.23	-0.23
δ	-1.43 ppm	-0.07 ppm	+0.14 ppm	+0.07 ppm

(c) Boundary conditions will have a small but real effect on the field shape calculations. Even with careful choices, a very "finite universe" applies to the computed field. This is another small systematic error to be removed by perturbation.

Cylindrically symmetric problems such as the g-2 ring can be calculated with POISSON in polar coordinates with the vertical axis at the center of the ring.

To date, only two dimensional (2D) calculations have been made. In the future it is planned to calculate in 3D. Small systematic changes in field shape will result.

The 2D version has the multipole fit built into the code. It is a very powerful tool. The 3D cylindrically symmetric field can also be fitted to a magnetic potential and a field fitting

code be introduced into the the program. This does not exist at present, and we see no need to develop it for our purposes. When the magnet design is almost final, the actual 3D field will be calculated. The difference in the 3D and 2D fields can be manually fitted to a 2D multipole expansion. It will involve long range effects, i.e., low order multipoles. By perturbation of the 2D magnet cross section, equal and opposite sign multipole changes will be put in the 2D field. This perturbed magnet will then when calculated in 3D give the correct uniform field shape.

This perturbation approach was verified on the earlier version of the g-2 ring, assuming a 5T superconducting air core magnet. The radius of curvature was much smaller (2m). Also there were no iron poles to localize the generation of the field shape. The deviation between the 2D and 3D field shapes was much larger than in the present design. Nonetheless, treating this deviation as a 2D perturbation to be corrected worked immediately. When the 2D geometry which gave an equal and opposite field error was computed in 3D coordinates, it produced the required uniform field.

(d) The 2D calculations also can give the correct return yoke cross sections and magnet weight of the actual (3D) magnet ring. This requires only straightforward calculations to keep the yoke reluctance the same in both cases.

The CERN magnet yokes were essentially polygons, composed of 40 straight magnet sections joined together at the poles. The present design assumes a continuous ring assembly to minimize the errors associated with magnet ends.

The magnet cross section was designed in two dimensions (2D). This was the cross section which appeared in the 1985 Proposal. This cross section was applied to the cylindrical ring (3D). This resulted in a considerable overestimate of the magnet ring weight and in fact would give a lower yoke reluctance than calculated.

A polygon design would have a total weight equal to the weight of the 2D cross section times a length of $2\pi \times 7$ meters.

In the continuous ring design, the bulk of the iron flux return yoke is at a considerably larger radius. The cross section should be scaled down accordingly. An angular section which is one meter long at the aperture center line radius of 7m should have the same weight as the 2D cross section for 1m of length.

This transformation was not performed on the engineering drawings in the 1985 Proposal, but the weight was corrected in the Table of Parameters.[1]

Consider first the block centered on the horizontal midplane. For the same reluctance, the 2D flux area = 3D flux area.

$$\text{i.e. } (r_2 - r_{in}) \times 2\pi \times 7m = (r_3^2 - r_{in}^2)\,\pi$$

where r_{in} = 755cm in Fig. 3 and r_3 = 804.4cm.

As a result, the outside radius of the ring, r_3, is smaller than the outside radius, r_2, of the 2D computed cross section.

A $\frac{1}{r}$ thickness adjustment should be applied to the top and bottom yoke pieces also, to produce the same reluctance as in the 2D calculations.

In the 1986 update, these corrections were applied. It was learned that cutting the corners off the yoke would result in real cost savings since the raw forgings could be so shaped. As described earlier, this was also incorporated into the design computations. The remaining small $\frac{1}{r}$ thickness variation in the top and bottom plates was then averaged out. Computed thickness perturbations verified this was not a significant factor.

Figure 3 is then the present ring cross section (3D) but with the same reluctance properties as the 2D cross section used in the computations. This correction, as well as the reduction in thickness of the yoke after inserting the air gap, resulted in the reduction in the magnet iron weight to 2/3 the original value.

Table IX lists the magnet steel parameters.

TABLE IX: Magnet Steel Parameters

Top Plate (also bottom)	Outside radius:	804.4 cm
	Inside radius:	672.0 cm
	Overall radial width:	132.4 cm
	Height (bottom surface):	22.0 cm
	Height (top surface):	76.0 cm
	Thickness (height):	54.0 cm
Midplane Block	Outside radius:	804.4 cm
	Inside radius:	755.0 cm
	Radial width:	49.4 cm
	Thickness (height):	44.0 cm
Gap behind poles	(effective)	1.0 cm
Pole width		56.0 cm
Pole thickness		12.0 cm
Aperture gap		18.0 cm
Total magnet weight		593.0 tonnes
Weight of top and bottom plates (assuming 45° sectors each)		29.2 tonnes (32.1 tons)

V. Calculations to be Performed

Many more magnet computations can be performed. Some can be usefully performed now to improve the design and increase perturbative capabilities. Others are required in an ongoing interaction to help the designers of coils, vacuum system, the measuring system, mechanical assembly, etc. Significant changes may be required because of these interactions once all aspects of the storage ring are well advanced in detailed design.

(a) Calculations of the forces and field multipole changes resulting from large changes in the locations of the magnet coils are needed. For example, the outer coils may have to be moved closer to the horizontal midplane because of possible interference of the dewar structure and the magnet iron. In fact the coil designers may finally need more space inside the C-shaped yoke for the SC coils and their support. This might require a slightly larger yoke.

(b) Vary the geometry of the pole to perturb the polar region such that all multipoles are ≤ 1 ppm. This will involve removing the present 32 ppm sextupole. The purpose of this is to enhance further our quantitative power to perturb all relevant multipoles.

This should be accomplished without significantly widening the poles and increasing the total flux crossing the horizontal midplane. Increasing the total flux in the aperture of the magnet and in the flux return would result in a larger and heavier magnet. The calculations indicate the present design is close to optimum in balancing field quality versus magnet weight.

(c) Although computed 2D to 3D effects are believed to be small and understood, we will rigorously set up and compute the magnet with cylindrical symmetry of radius 7 meters.

(d) Vary the geometry of the air gap behind the poles. Explore the moving of iron in this air gap to generate quadrupole and possibly sextupole harmonic terms.

(e) Explore the fine tuning of quadrupole field errors by adding iron shims to the inside yoke surfaces at r = 672 cm.

(f) Explore control of quadrupole and sextupole harmonics by small shims on the side of the poles.

(g) Special magnet (high μ) steels for possible location at pole tip edges can be studied. Also weakly parametric shim materials might be calculated.

(h) An extensive effort on computing correcting coil locations for dipole, quadrupole, sextupole, etc. as needed. Skew multipoles are also required.

(i) When the experimental properties of the actual iron used in the ring are known, final perturbations will be required.

(j) Finally, during the construction and test stage, calculations will be a great aid to empirical shimming.

VI. Environmental Influences on the Magnet

The cylindrical symmetry assumed in the magnet calculations will be sometimes violated. Calculations can aid in some but not all these problems.

(a) A mechanically stable foundation with maximum vibration suppression is required. Magnet iron and coil supports should also be concerned with vibration. For example, relative motion of coils and iron is not desirable.

(b) The housing should provide both flux and thermal screening from the environment. The saturation magnetization (M_s) of iron varies by $\sim 1 \times 10^{-4}$ per °C. At CERN they controlled the temperature to 1°C. The calculations in Table II indicate that a $M_s = 1 \times 10^{-4}$ change is acceptable. However, sudden changes and gradients of temperature are undesirable and could cause differential forces and distortion. Isothermal steel is very desirable.

(c) Stable magnet support, with accurate and easy survey and adjustment capability are essential for the "continuity" of the ring. If the 45° sectors open up azimuthally or are displaced vertically, field errors will arise.

(d) A very reliable cryogenic system with maximum redundancy of components to ensure uninterrupted running is very important. This will permit long and elaborate charging cycles and continuous current operation as desired for magnet measurement and physics runs.

(e) The injector system will perturb the "good field" aperture region. This will either be a dynamic distortion, as was the case at CERN or with possible muon injection, or else a static field distortion with superconducting injection magnets used. Injection will cause a major distortion in the magnetic field.

This interaction is partially amenable to computations and must be understood and probably corrected in situo for 0.1 ppm precision.

References

1. AGS Proposal. A new Precision Measurement of the Muon g-2 Value at the Level of 0.35 PPM. V.W. Hughes et al. September 1985.

2. AGS Proposal 821, September 15, 1986 (same title).

3. R. Holsinger (LANL), private communication, 1976. J. Galayda and R. Thern installed the CDC version of POISSON at BNL.

4. Final Report of the CERN Muon Storage Ring. J. Bailey et al. Nuclear Physics B150 (1979) 1-75.

5. H. Drumm, "The Storage Ring Magnet of the Third Muon (g-2) Experiment at CERN," NIM 158, pp. 347-362 (1979).

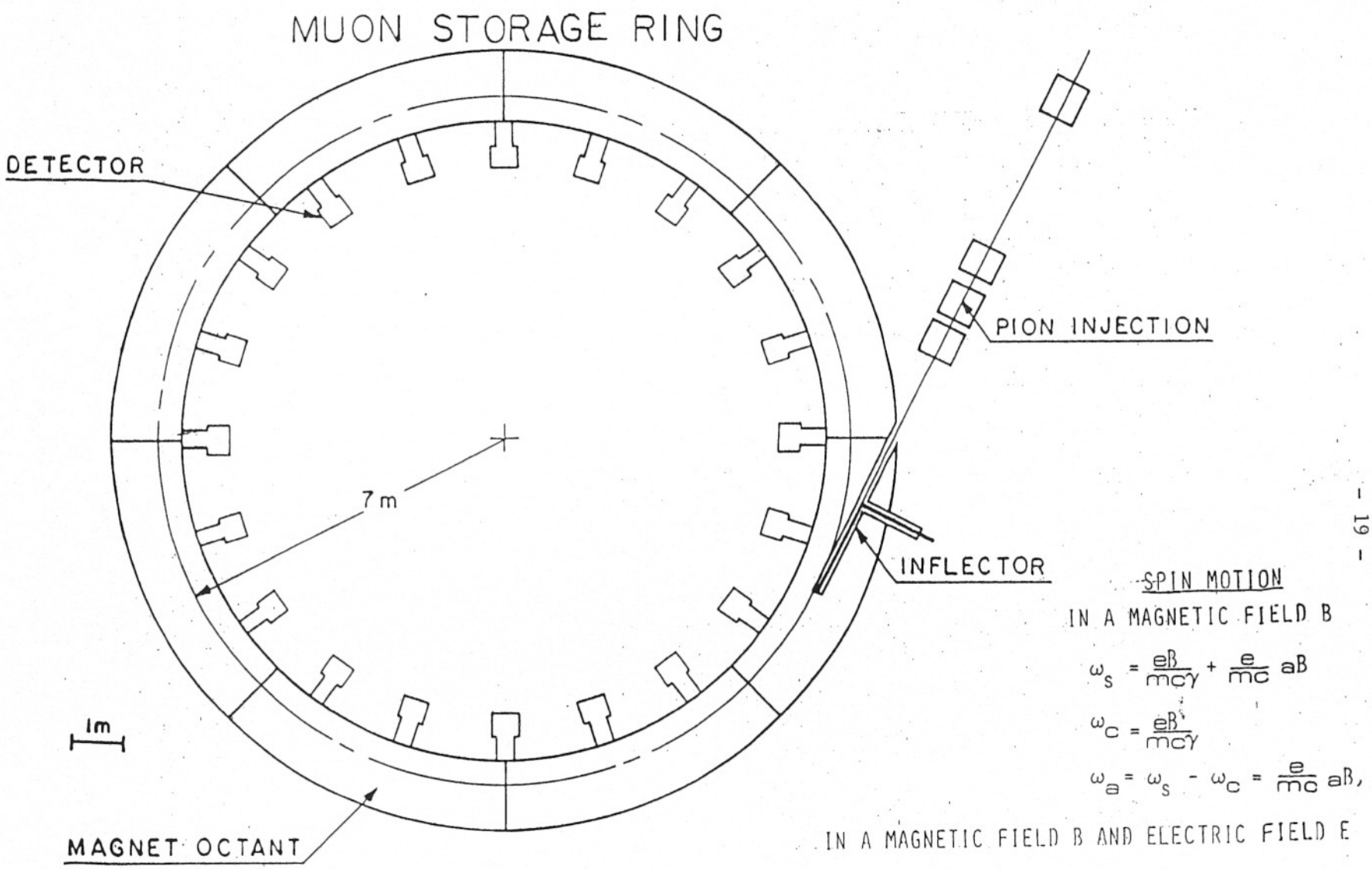

SPIN MOTION

IN A MAGNETIC FIELD B

$$\omega_s = \frac{eB}{mc\gamma} + \frac{e}{mc} aB$$

$$\omega_c = \frac{eB}{mc\gamma}$$

$$\omega_a = \omega_s - \omega_c = \frac{e}{mc} aB,$$

IN A MAGNETIC FIELD B AND ELECTRIC FIELD E

$$\omega_a = \frac{d\theta_R}{dt} = \frac{e}{mc}\left[aB + \left(a - \frac{1}{\gamma^2 - 1}\right)|\vec{\beta} \times \vec{E}|\right]$$

$$\gamma_{MAGIC} = 29.3$$

Fig. 1 SCHEMATIC LAYOUT OF EXPERIMENT

RING MAGNET - CROSS SECTION

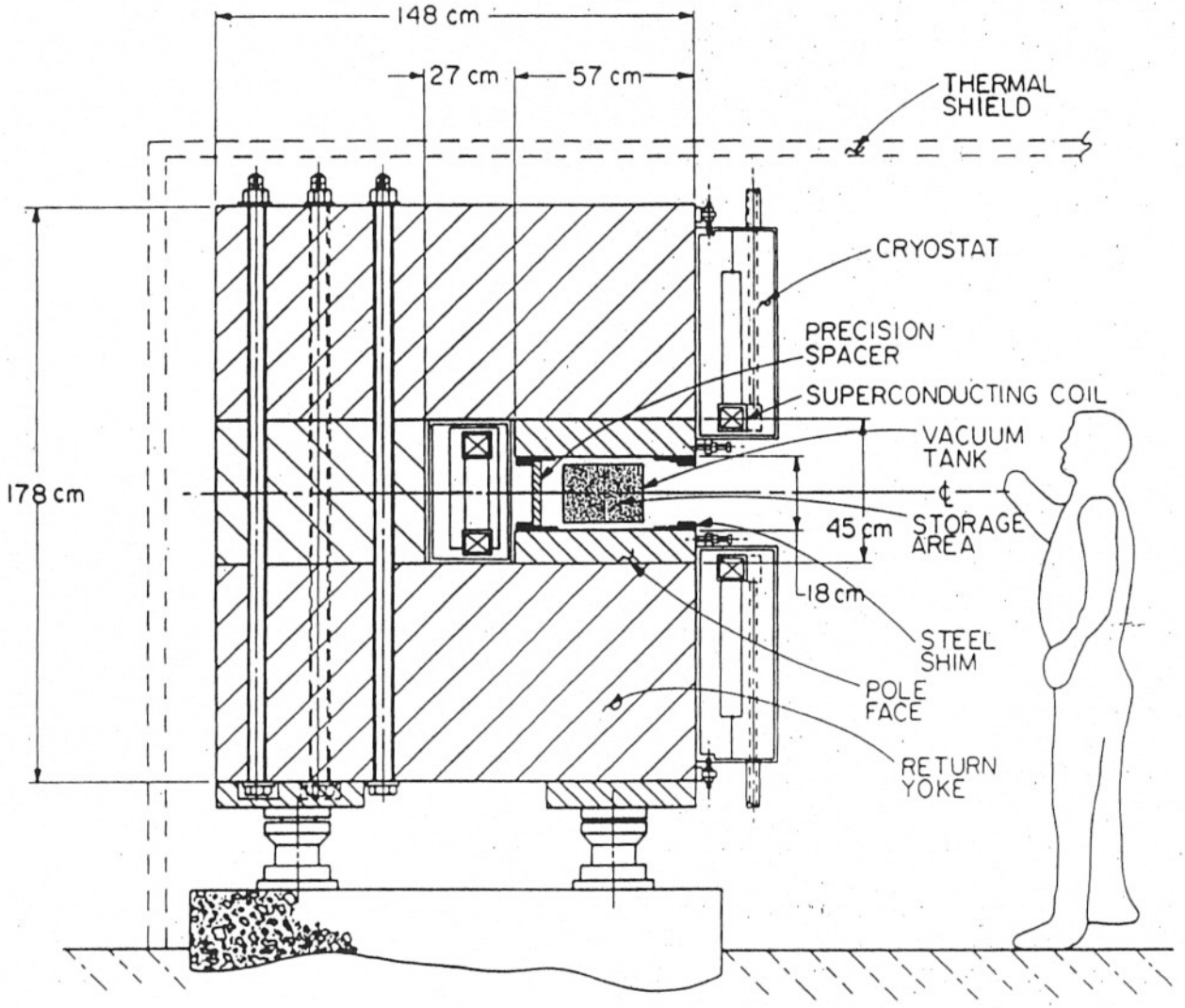

Fig. 2 STORAGE RING MAGNET (1985)

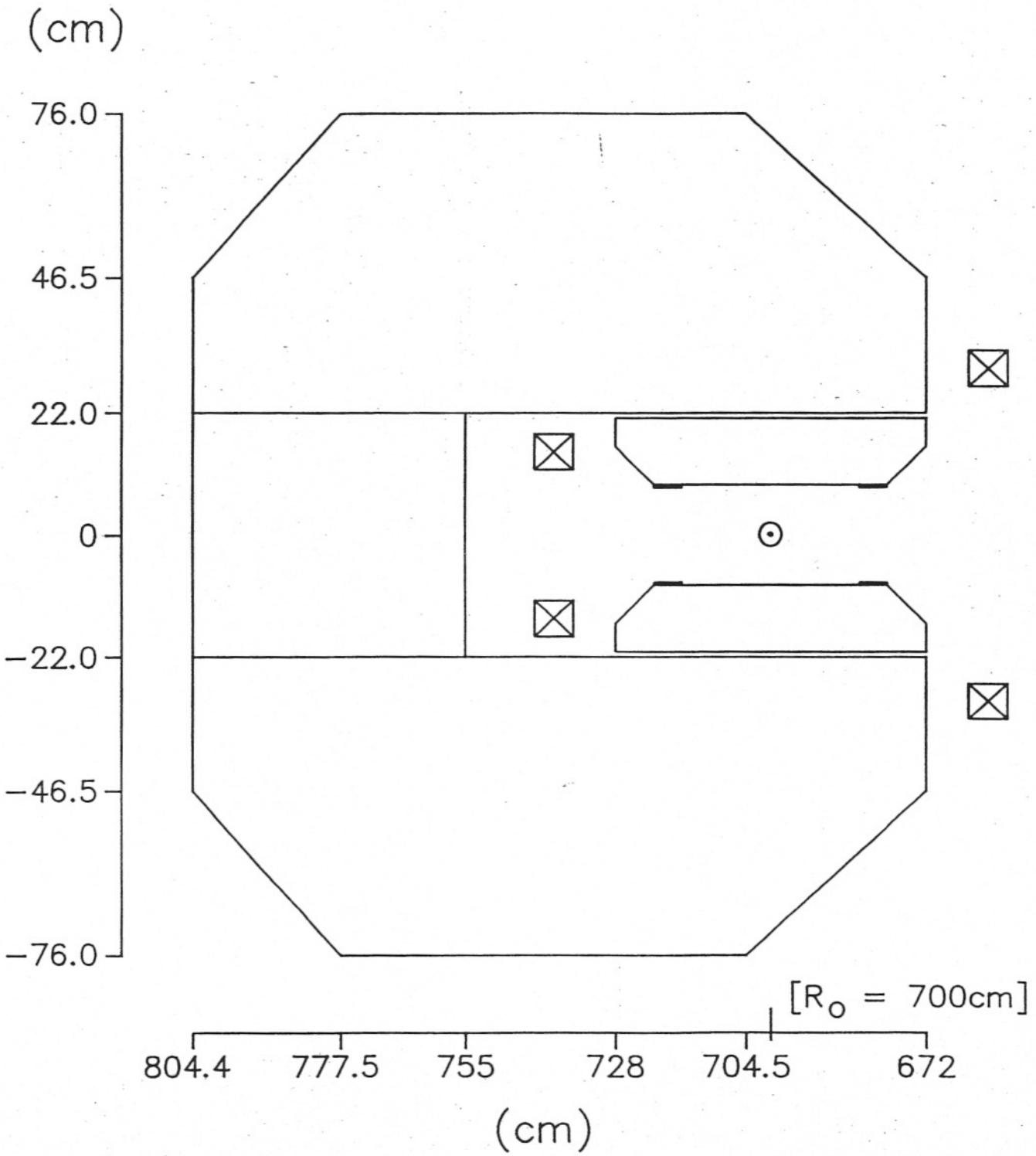

Fig. 3 MAGNET CROSS SECTION (1986)

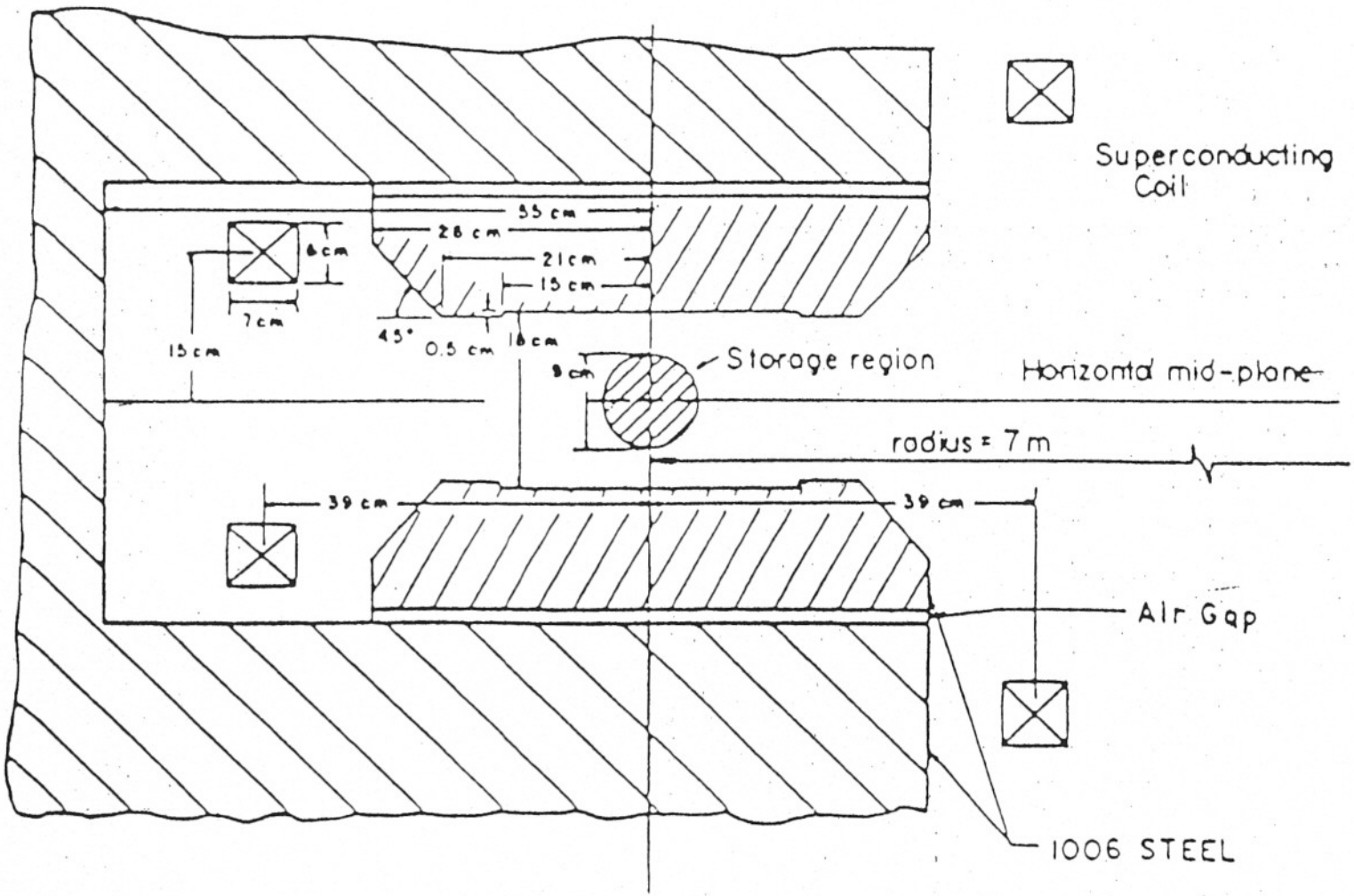

Fig. 4 MAGNET POLE REGION (1986)

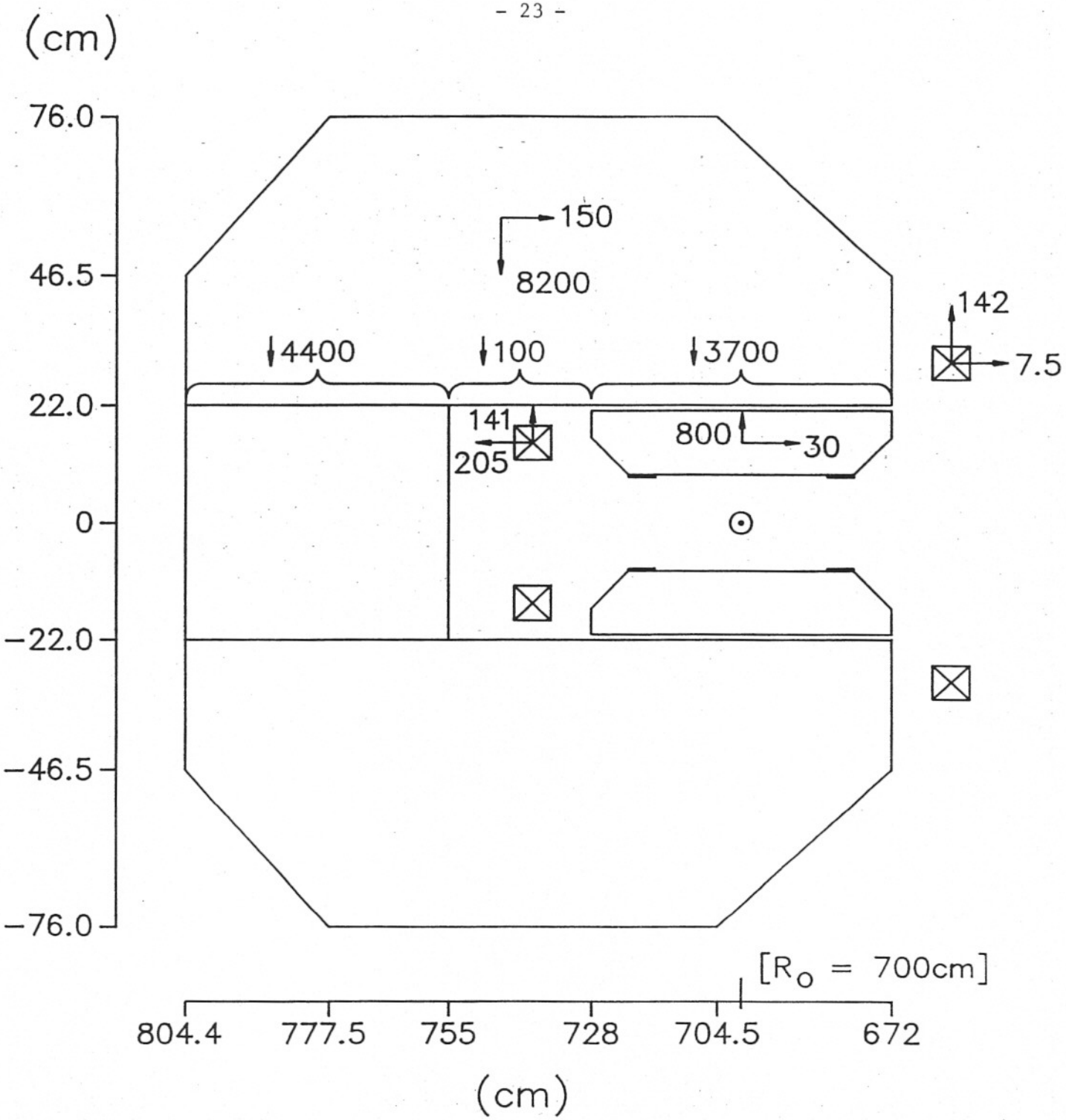

FORCES EXPRESSED IN LB./LINEAR INCH AT R = 7.0 METERS

Fig. 5 FORCES AT B_o = 14.7 kG

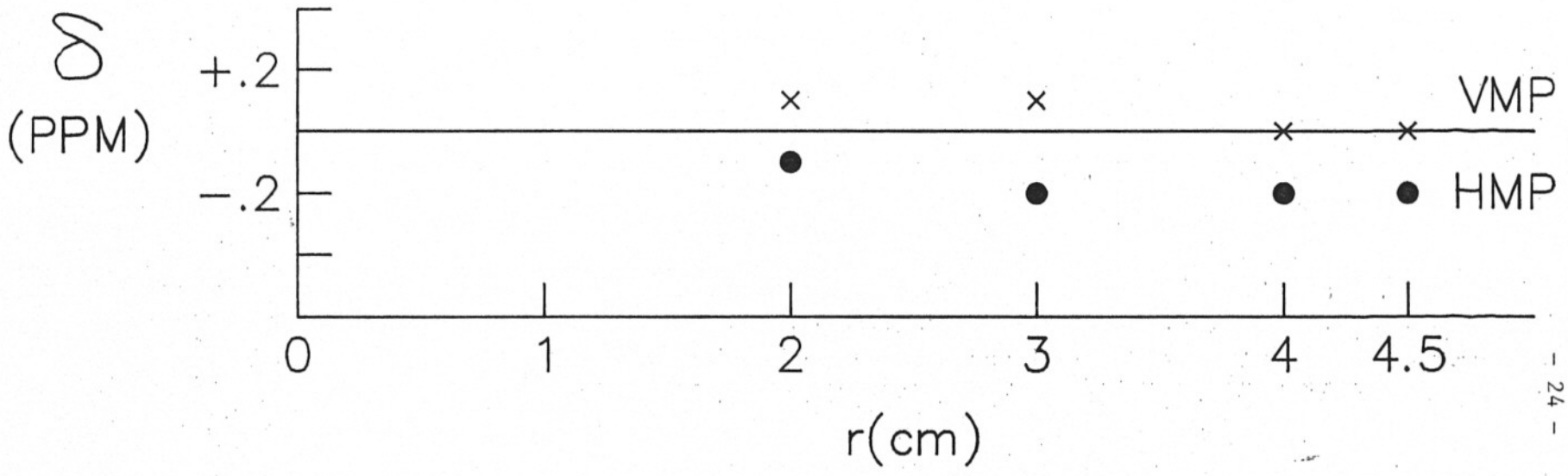

δ ≡ MULTIPOLE RECONSTRUCTED FIELD − COMPUTED FIELD

Fig. 6 δ vs. r FOR HORIZONTAL AND VERTICAL MIDPLANES